Uncertainty-fully-aware Coordinated Dispatch of Integrated Electricity and Heat System

Skalyga, Mikhail; Wu, Qiuwei; Zhang, Menglin

Published in:
Energy

Link to article, DOI:
10.1016/j.energy.2021.120182

Publication date:
2021

Document Version
Early version, also known as pre-print

Uncertainty-fully-aware Coordinated Dispatch of Integrated Electricity and Heat System

Mikhail Skalyga[a,b], Qiuwei Wu[a,*], Menglin Zhang[a]

[a] *Center for Electric Power and Energy, Department of Electrical Engineering, Technical University of Denmark (DTU), 2800 Kgs. Lyngby, Denmark*
[b] *Division of Electric Power and Energy Systems, School of Electrical Engineering, KTH Royal Institute of Technology, Teknikringen 33, 100 44 Stockholm, Sweden*

Abstract

The power system operators are facing significant challenges in the operation due to the increasing penetration level of renewable energy sources (RESs). The flexibility from the district heating system (DHS) is attracting considerable interest to deal with RES uncertainty. This paper formulates a distributionally robust chance-constrained (DRCC) optimization model of the integrated electricity and heating system (IEHS) dispatch to hedge the uncertainty of RES and exploit the flexibility of the DHS. In particular, the uncertainty from the electrical power system (EPS) is propagated to the DHS so that both systems can respond to the uncertainty of RES. The uncertainty of the wind power is modeled by an ambiguity set, which defines a family of probability distributions with the same first and second-moment property. Real-time regulation actions of both the EPS and DHS to respond to the wind power forecast errors are modeled through the data-driven affine control policies. To achieve computational tractability, the proposed DRCC model is reformulated as a second-order cone program (SOCP). The simulation results tested on the integrated six-bus and seven-node system demonstrate that the proposed DRCC model outperforms the chance-constraints dispatch based on Gaussian distribution for the secure operation of the IEHS.

Keywords: Integrated electricity and heating systems, distributionally robust optimization, affine policies, uncertainty modeling, second-order cone program

Nomenclature

Indexes and Sets

Λ^{N+} Set of nodes with a single pipe starting

*Corresponding author
Email address: qw@elektro.dtu.dk (Qiuwei Wu)

Λ^{N-} Set of nodes with a single pipe ending

Λ^{N} Set of nodes

Λ^{P} Set of pipes

Θ_n^{CHP} Set of CHPs at node n, $\Theta_n^{CHP} \in \Theta_n^{HS}$

Θ_n^{HL} Set of heat loads at node n

Θ_n^{HP} Set of heat pumps at node n, $\Theta_n^{HP} \in \Theta_n^{HS}$

Θ_n^{HS} Set of heat sources (HS) at node n

$\Theta_n^{P,IN}$ Set of indices of pipes ending at node n

$\Theta_n^{P,OUT}$ Set of indices of pipes starting at node n

i Index of conventional generators

k Index of transmission lines

l Index of thermal loads

n Index of nodes

p Index of pipes

s Index of heat sources

t Index of operating hours

Parameters

λ_p Thermal loss coefficient in pipe $[J \times m^{-2} \times s^{-2}/^{\circ}\mathrm{C}]$

$\overline{\tau}_{p,t}^{S}, \overline{\tau}_{p,t}^{R}$ Maximum time delays in supply and return pipes p $[h]$

$\overline{F}_s$ Maximum fuel consumption of CHP unit [MW]

$\overline{R}_s^C, \underline{R}_s^C$ Rump-up and -down capability of CHP unit [MW]

$\overline{R}_i^G, \underline{R}_i^G$ Rump-up and -down capability of generators [MW]

ρ Water density $[\mathrm{kg}/m^3]$

ρ_s Heat-to-Electricity output ratio of the extraction CHP

$\rho_s^H, /\rho_s^E$ Heat/Electricity-to-fuel ratio of the extraction CHP

$\underline{H}_s^{HS}, \overline{H}_s^{HS}$ Minimum and maximum heat supply from HS unit [MW]

$\underline{P}_i^G, \overline{P}_i^G$ Minimum and maximum real power output of generators [MW]

$\underline{T}_n^R, \overline{T}_n^R$ Minimum/maximum temperature at node n in the return network [°C]

$\underline{T}_n^S, \overline{T}_n^S$ Minimum/maximum temperature at node n in the supply network [°C]

C Specific water capacity [J/kg°C]

c_s^e, c_s^h Cost coefficients for CHP [$/MWh]

c_i^g Operation cost of convectional generators [$/MWh]

COP_s Coefficient of performance of heat pump (HP)

$H_{l,t}^L$ Heat demand [MW]

L_p Length of pipe p [m]

$m_{l,t}^{HL}$ Mass flow rate of heat load l [kg/s]

$m_{s,t}^{HS}$ Mass flow rate of heat station s [kg/s]

$m_{p,t}^S, m_{p,t}^R$ Mass flow rate of pipeline p [kg/s]

P_t^D Electric demand vector [MW]

P_t^f Wind power forecast vector [MW]

P^L Line transmission capacity vector [MW]

R_p Radius of pipe p [m]

Decision Variables

α_t^C CHP participation factor

α_t^G Generator participation factor

α_t^H HP participation factor

β_t^H Heat station participation factor

γ_t^R Return nodal temperature participation factor

γ_t^S Supply nodal temperature participation factor

$\tau_{p,t}^S, \tau_{p,t}^R$ Time delays in supply and return pipes p [h]

$H_{s,t}^{HS}$ Heat supply from heat station unit s [MW]

$P_{i,t}^G$ Day-ahead power dispatch of generator i [MW]

$P_{s,t}^C$ Day-ahead power dispatch of CHP unit s [MW]

$P_{s,t}^{HP}$ Power consumption of HP [MW]

$T_{p,t}^{R,end}$ Temperature at the end node of pipe p in the return network [°C]

$T_{p,t}^{R,start}$ Temperature at the start node of pipe p in the return network [°C]

$T_{n,t}^{R}$ Temperature of a node n in the return network [°C]

$T_{p,t}^{S,end}$ Temperature at the end node of pipe p in the supply network [°C]

$T_{p,t}^{S,start}$ Temperature at the start node of pipe p in the supply network [°C]

$T_{n,t}^{S}$ Temperature of a node n in the supply network [°C]

1. Introduction

Flexibility provision by the district heating system (DHS) has been seen as a prominent solution for operating wind dominated power systems [1]. In Denmark, where the goal is to achieve a 100 % renewable energy system by 2050, the DHS will be expanded [2] to achieve the goal. Combined heat and power (CHP) units are considered to be the main source of the thermal energy in the DHS supplying up to 68 % of the heat and up to 57 % of the power in Denmark [3]. Generally, flexibility is provided by the fast ramp generators, e.g., gas-fired power plants. However, increasing penetration of the RESs has brought the need for the other sources of flexibility with less marginal cost [4]. Moreover, power-to-heat technology in combination with existing CHP units is seen beneficial to reduce the wind curtailment and a way to integrate DHS and EPS into one energy system [2, 5, 6]. Thus, the integration of the EPS and DHS has been extensively studied to unlock the required flexibility.

In recent years, there has been growing interest in the IEHS. In [7], a linear centralized dispatch model for the IEHS, including CHP, electrical boilers, and heat storage was proposed. The study shows that both electric boilers and heat storage increase the flexibility of the CHP unit. However, because of the heat losses in the pipes and thermal dynamics, the amount of energy that is scheduled in the day-ahead may not be delivered to the load and therefore the dispatch may not be implementable. Considering the district heating network (DHN) in the economic dispatch or optimal power flow problem brings additional constraints into the optimization problem. In [8], optimal operation of the IEHS was investigated considering network constraints in both systems. The resulting model is a large-scale non-linear optimization problem (NLP), which is solved with a decomposition algorithm. It is shown that interaction between two systems helps to reduce the wind power curtailment, energy losses, and operational cost.

Thermal storage in the district heating pipes improves the flexibility of the DHS and allows the utilization of more wind power without creating new storage capacities. For example, in [9], the integrated heat and power dispatch model was proposed accounting for the thermal inertia of the DHS. Since the circulation of mass flows remains constant, the final model is a large-scale linear

program (LP) that shows improvement in the operational flexibility of the CHP. Additionally, in [10], combined heat and power dispatch model was formulated to exploit the energy storage capability of the DHS. Due to the variable mass flow rates, the obtained model is a large-scale mixed-integer nonlinear program (MINLP). The model is solved with an integrative Bender's decomposition algorithm. These types of programs are computationally hard to solve and the final solution might be locally optimal. The authors of [11] overcame this issue by introducing a Taylor series expansion of the solution for the heat propagation equation and applying convex relaxations algorithms. The original non-convex problem was relaxed into a mixed-integer linear program (MILP) and solved with a commercial solver. A more recent study [12] also focused on linearization and convexification of the nonlinear DHS constraints. The entire economic dispatch problem was modeled as a mixed-integer conic program (MICP) accounting for not only changes of the mass flow rates, but also the direction. The model focused on the distribution level of the EPS and DHS, and therefore thermal dynamics were not accounted for.

The residential buildings' thermal inertia can be utilized for thermal energy storage purposes [13, 14, 15]. Heating for residential buildings could represent 80-90 % of the overall heat demand in the winter period [14] and it is seen as an additional source of flexibility. Ref. [16] proposed an integrated electricity and heat demand-side management model without a heating network to increase wind power integration in China. The resulting MINLP is solved with an outer approximation and equality relaxation algorithm and showed an increment in the wind power integration. The model can be exported to the other countries as long as the wind power, CHP, and electrical HPs exist in the power grid. Additionally, several studies have been published to consider both the thermal inertia of the residential buildings and district heat pipes storage capacity in the optimal operation models to further increase flexibility [15, 17, 18]. Ref [17] modeled transmission delay through the velocity of the thermal water and building storage with the indoor temperature of the buildings connected to the heat exchanger stations. The proposed model achieved a higher utilization rate of wind power at lower operation costs. In [18], the authors considered both pipelines' thermal dynamics and buildings' thermal inertia to improve the system's operational flexibility. Several simulation tests demonstrated that the proposed model has a good performance on power and heat decoupling.

One of the main challenges to operate EPSs with large amounts of RESs is their stochastic nature [19]. The lack of perfect information results in difficulties for the system operator on how to make the decisions before operation. The above-mentioned references have focused only on dispatching the IEHSs based on the deterministic point forecasts. Traditionally, two approaches have been used in the market-clearing and system operation problems in the presence of uncertainty. These are stochastic programming [20] and robust optimization [21]. In stochastic programming, the objective function minimizes the system cost in day-ahead and the *expected* system cost in real-time. The uncertain input data is represented by a set of scenarios with sum of probabilities adding to 1. In [22], the stochastic programming was applied to dispatch CHP units in the

micro-grid with a wind turbine and photovoltaic units. The uncertainties from the electrical market price, solar radiation, and wind speed were considered using a scenario-based method. Authors of [23] used stochastic optimization to provide day-ahead scheduling of integrated multi-energy systems. A robust optimization approach models uncertainty through uncertainty sets and the final solution is optimal for the worst-case realization of the resource cost. The problem formulated usually as a three-level min-max-min optimization problem, which is a three-level game against "nature". The robust optimization method was applied to dispatch IEHSs in [24, 25, 26].

Stochastic programming heavily relies on the amount and quality of generated scenarios. For the large scale systems, the amount of scenarios grows significantly and the solution of the problem becomes computationally demanding. The scenario reduction methods could reduce the number of scenarios, but if the scenario that has not been foreseen arise, the decision might not be implementable. At the same time, the worst-case realization in the robust optimization method happens rarely, and therefore the solution is too conservative and costly. Recent developments in the field of distributionally robust optimization (DRO) could remedy the difficulties mentioned above [27]. In DRO, a decision maker uses available data to build an ambiguity set, which is a family of probability distributions, and the solution is robust against the worst possible distribution inside the ambiguity set. The model is a three-level min-max-min problem to minimize the worst-case *expected* cost. However, in this game, "nature" selects a distribution within the ambiguity set to harm the decision maker as much as possible [28]. DRO has many applications in the field of power system operation. For example, the DRO method was applied in the optimal power flow problems [29, 30, 31], unit commitment problem [32], and generation expansion planning problem [33] to handle the uncertainty in power systems. In the IEHS systems, the approach was used in [34, 35] to determine the optimal day-ahead unit commitment, and energy and reserve dispatch respectively. Refs [36, 37] applied the approach in the integrated electricity and natural gas system for considering the uncertainty in the natural gas system network.

The contributions of this work are summarized as follows:

- Given the advantages of the DRO method, a DRCC optimization model for the IEHS operation is proposed. Unlike the method in [27], where historical samples are used to construct scenarios to describe possible wind power output realizations, historical data are used to obtain statistical information about the probability distribution of the uncertainty and the distribution is considered to be continuous. Moreover, the problem is solved directly without decomposition algorithms.

- Real-time response of the DHS to the uncertainty is modeled with the affine polices, providing feasible operation of the system in real-time. Although the uncertainty in the DHS have been investigated in the most recent previous studies [34, 35], approach proposed is based on chance-constraint programming, which provides the system operator a tool to control the risk of planning decisions.

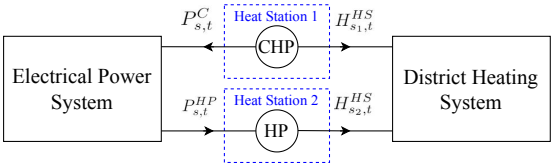

Figure 1: Heat station units.

- Spatial and temporal correlations of the wind power forecast errors are accounted for. The model requires information only about the first and second moments of the uncertainty. In the model, the uncertainty does not follow any particular type of probability distribution and apply tractable reformulations of chance-constraints to solve the model with commercial solvers.

The remaining parts of the paper is organized as follows. Section 2 introduces the deterministic optimal operation of the IEHS. In Section 3, the deterministic formulation was extended to include the uncertainty from the wind power forecast. Section 4 provides tractable second-order cone reformulation of the chance-constraint program. In section 5, a case study is presented and results are analyzed. Finally, our conclusions are drawn in Section 6.

2. Deterministic Integrated Electricity and Heat System Operation

2.1. DHS structure

We consider N^c number of extraction CHP units that co-generate power and thermal energy. We also incorporate N^h number of HPs into the system to increase operational flexibility. HPs consume power to produce thermal energy. These heat sources make up $N^{HS} = N^c + N^h$ number of heat stations that supply heat to the DHS, as shown in Fig. 1. Radially structured DHN with N nodes distributes energy through P supply pipelines to the L heat loads. In the transmission system, heat loads are referred to as heat-exchanger stations, which, in turn, procure heat power for the distribution network. The water passed through the heat exchanger is cooled down and transferred back to the heat stations via P return pipes. One transmission system can cover several distributions systems in different areas [38].

2.2. EPS structure

The EPS includes G number of conventional generation units that can produce electrical power only. We assume W number of the wind power plants, whose power production is uncertain. The power flows through the network that consists of B buses and K lines to meet D electrical demands. The index represents the element of the vector with a corresponding dimension. For example, we denote the vector $P^G_t \in \mathbb{R}^G$ and $P^G_{i,t}$ represents its element. Moreover, $\mathbf{1}$ is a vector of ones.

2.3. Model assumptions

1. We focus on the IEHS at the transmission level, and hence we use DC model of the EPS, which is a linear approximation of the power flow equations.
2. Renewable energy sources are scheduled at their forecasted power production with zero marginal cost.
3. DHS could be operated under different control strategies, such as constant mass flow and constant temperature, variable mass flow and constant temperature, constant mass flow and variable temperature, variable mass flow, and variable temperature. The difference between the last two could be seen in [25]. We assume constant mass flow and variable temperature strategy since the model has more practical meaning and is often used in the integrated energy systems study [25, 26, 39]. Near-optimal values of mass flow rates could be found with a two-step hydraulic-thermal decomposition algorithm [40] to cut down heat losses and reduce operational cost.
4. It is assumed that the IEHS operator dispatches the system based on the forecasted wind power output and demand. In real-time, the variability of the demand is much less, and therefore we neglect the uncertainty of the load forecast.

2.4. EPS constraints

$$\mathbf{1}^T P_t^G + \mathbf{1}^T P_t^C + \mathbf{1}^T P_t^f = \mathbf{1}^T P_t^D + \mathbf{1}^T P_t^{HP}, \forall t \tag{1a}$$

$$-P^L \leq C^G P_t^G + C^W P_t^f + C^C P_t^C - C^D P_t^D - C^{HP} P_t^{HP} \leq P^L, \forall t \tag{1b}$$

$$\underline{P}^G \leq P_t^G \leq \overline{P}^G, \forall t \tag{1c}$$

$$P_t^G - P_{t-1}^G \leq \overline{R}^G, \forall t+1 \tag{1d}$$

$$P_{t-1}^G - P_t^G \leq \underline{R}^G, \forall t+1 \tag{1e}$$

$$P_t^C - P_{t-1}^C \leq \overline{R}^C, \forall t+1 \tag{1f}$$

$$P_{t-1}^C - P_t^C \leq \underline{R}^C, \forall t+1 \tag{1g}$$

Constraint (1a) enforces power balance in the EPS. Constraint (1b) limits the power flow along the lines. Matrices $C^G \in \mathbb{R}^{K\times G}$, $C^C \in \mathbb{R}^{K\times N^c}$, $C^W \in \mathbb{R}^{K\times W}$, $C^D \in \mathbb{R}^{K\times D}$, and $C^{HP} \in \mathbb{R}^{K\times N^h}$ have all information about the transmission network structure and its physical characteristics. The matrices are obtained by multiplying Power Transfer Distribution Factor [41] with mapping matrices. Constraint (1c) ensures conventional generators' limits, while (1d) and (1e) constrain their ramping capability. Finally, (1f) and (1g) restrict power ramping of CHP units.

2.5. DHS constraints

Modeling of the DHS follows [11].

$$H_{s,t}^{HS} = Cm_{s,t}^{HS}\left(T_{n,t}^{S} - T_{n,t}^{R}\right), \forall n \in \Lambda^{N}, \forall s \in \Theta_{n}^{HS}, \forall t \tag{2a}$$

$$\underline{H}_{s}^{HS} \leq H_{s,t}^{HS} \leq \overline{H}_{s}^{HS}, \forall s \in \Theta_{n}^{HS}, \forall t \tag{2b}$$

$$H_{l,t}^{L} = Cm_{l,t}^{HL}\left(T_{n,t}^{S} - T_{n,t}^{R}\right), \ \forall n \in \Lambda^{N}, \forall l \in \Theta_{n}^{HL}, \forall t \tag{2c}$$

$$\begin{aligned} \sum_{p \in \Theta_{n}^{P,IN}} m_{p,t}^{S} T_{p,t}^{S,end} &= T_{n,t}^{S} \sum_{p \in \Theta_{n}^{P,IN}} m_{p,t}^{S}, \ \forall n \in \Lambda^{N}, \forall t \\ \sum_{p \in \Theta_{n}^{P,OUT}} m_{p,t}^{R} T_{p,t}^{R,end} &= T_{n,t}^{R} \sum_{p \in \Theta_{n}^{P,OUT}} m_{p,t}^{R}, \ \forall n \in \Lambda^{N}, \forall t \end{aligned} \tag{2d}$$

$$\begin{aligned} T_{n,t}^{S} &= T_{p,t}^{S,start}, \ \forall n \in \Lambda^{N}, \ \forall p \in \Theta_{p}^{P,OUT}, \forall t \\ T_{n,t}^{R} &= T_{p,t}^{R,start}, \ \forall n \in \Lambda^{N}, \ \forall p \in \Theta_{p}^{P,IN}, \forall t \end{aligned} \tag{2e}$$

$$\begin{aligned} T_{n,t}^{S} &= T_{p,t}^{S,end}, \ \forall n \in \Lambda^{N-}, \ \forall p \in \Theta_{p}^{P,IN}, \forall t \\ T_{n,t}^{R} &= T_{p,t}^{R,end}, \ \forall n \in \Lambda^{N+}, \ \forall p \in \Theta_{p}^{P,OUT}, \forall t \end{aligned} \tag{2f}$$

$$\underline{T}_{n}^{S} \leq T_{n,t}^{S} \leq \overline{T}_{n}^{S}, \ \underline{T}_{n}^{R} \leq T_{n,t}^{R} \leq \overline{T}_{n}^{R}, \ \forall n \in \Lambda^{N}, \forall t \tag{2g}$$

$$\begin{aligned} T_{p,t}^{S,end} &= T_{p,t-\tau_{p,t}^{S}}^{S,start}\left(1 - \tfrac{2\lambda_{p}}{C\rho R_{p}}\tau_{p,t}^{S}\right), \forall p \in \Lambda^{P}, \forall t \\ T_{p,t}^{R,end} &= T_{p,t-\tau_{p,t}^{R}}^{R,start}\left(1 - \tfrac{2\lambda_{p}}{C\rho R_{p}}\tau_{p,t}^{R}\right), \forall p \in \Lambda^{P}, \forall t \end{aligned} \tag{2h}$$

Equation (2a) is the heat power produced by each heat station and it is bounded by (2b). Equation (2c) defines the thermal power consumed by heat loads. Constraints (2d) are the temperature mixture equations for the return and supply network. Constraint (2e) ensures that the temperature at the beginning of a pipe leaving a node is equal to the mixture temperature at that node. Constraints (2f) impose the equality of ending temperature of a single pipe at a node and the nodal temperature at that node. Constraints (2g) restrict the nodal temperatures within their operational bounds. Equations (2h) are approximated solutions of the heat propagation equation [11] which accounts for temperature dynamics and heat losses in the pipes. In the transmission-scale DHS, parameters of the pipes affect the thermal inertia and the system needs relatively long time to achieve the thermal equilibrium. The discrete time delays $\tau_{p,t}^{S}$ are calculated as the solution of the following optimization problem:

$$\min_{\phi \in \{0,\ldots,\overline{\tau}_{p}^{S}\}} \phi$$

subject to:

$$\frac{\sum_{t-\phi}^{t} m_{p,t}^{S}}{\pi R_p^2 \rho} \Delta t \geq L_p, \forall p \in \Lambda^P, \forall t$$

The problem above is a MILP and is solved before running the operational model. Discrete time delays $\tau_{p,t}^R$ for the return network computed similarly.

2.6. Linking units

$$\begin{aligned} & P_{s,t}^C \geq r_s H_{s,t}^{HS}, \ \forall s \in \Theta_n^{CHP}, \forall t \\ & 0 \leq \rho_s^E P_{s,t}^C + \rho_s^H H_{s,t}^{HS} \leq \overline{F}, \ \forall s \in \Theta_n^{CHP} \forall t \end{aligned} \tag{3a}$$

$$H_{s,t}^{HS} = COP_s P_{s,t}^{HP}, \ \forall s \in \Theta_n^{HP}, \forall t \tag{3b}$$

Equations (3a) are approximations of the feasible operation region of the extraction CHP unit [11] and equation (3b) defines the ratio between consumed power and produced heat in the HP. These units provide interconnection between the heating and electrical side.

2.7. Objecive function

$$\sum_t (c^g)^T P_t^G + (c^e)^T P_t^C + (c^h)^T H_t^{HS} \tag{4}$$

Objective function (4) minimizes total operation cost of the IEHS. As a result, the full model is a linear optimization problem

$$\min (4)$$

subject to: (1a)-(3b) constraints, over the set of optimization variables

$$\begin{aligned} \Xi = \{ & T_{p,t}^{S,start}, T_{p,t}^{S,end}, T_{p,t}^{R,start}, T_{p,t}^{R,end}, T_{n,t}^S, T_{n,t}^R, \\ & H_{s,t}^{HS}, P_t^C, P_t^{HP}, P_t^G \} \end{aligned}$$

3. Uncertainty-aware Integrated Electricity and Heat System Operation

3.1. Uncertainty modeling

In real-time uncertain wind power generation is modeled as $P_t^f - \xi_t, \forall t$, where $\xi_t \in \mathbb{R}^W$ - is a vector of the forecast error. Random variable ξ_t follows unknown probability distribution $\mathbb{P}_{\xi_t}$ and has a mean $\mu_t \in \mathbb{R}^W$ and a covariance matrix $\Sigma_t \in \mathbb{R}^{W \times W}$. Covariance matrix $\Sigma_t \in \mathbb{R}^{W \times W}$ considers the spatial correlation of corresponding forecast errors between W wind parks at each hour t. Given N number of training data samples we calculate empirical mean $\mu_t = \frac{1}{N} \sum_{l=1}^{N} \xi_t^l$

and covariance matrix $\Sigma_t = \frac{1}{N}\sum_{l=1}^{N}(\xi_t^l - \mu_t)(\xi_t^l - \mu_t)^T$ and build ambiguity set $\mathcal{D}_{\xi_t}$ for each hour t such as

$$\mathcal{D}_{\xi_t} := \{\mathbb{P}_{\xi_t} \in \mathcal{P}' : \mathbb{E}_{\mathbb{P}_t}[\xi] = \mu_t, \mathbb{E}_{\mathbb{P}_t}[(\xi_t - \mu_t)(\xi_t - \mu_t)^T] = \Sigma_t\} \tag{5}$$

where $\mathcal{P}'$ is a family of all distributions with the same mean μ_t and covariance Σ_t. In the literature, this type of ambiguity set is referred to as moment-based. Another type of ambiguity set widely used is metric-based. It is defined as a ball in the space of probability distributions and uses the notion of a "distance" from a reference distribution [42, 43]. Even though the metric-based ambiguity sets offer stronger out-of-sample performance, the moment-based ones display better tractability properties [43]. Specifically, DRO models with moment-based ambiguity sets are more tractable than the corresponding stochastic models. Moreover, DRO models with metric-based ambiguity sets are computationally harder than their stochastic counterparts [43].

3.2. Affine Policies

Due to imperfect forecasts of the wind power output, deviation from the original forecast may occur in real-time. Taking into account the uncertainty from the forecast errors, we model the real-time response of controllable generation units via affine control policies [36]. The response of controllable generation units is expressed as follows

$$\tilde{P}_t^G = P_t^G + \alpha_t^G(\mathbf{1}^T\xi_t), \forall t \tag{6a}$$

$$\tilde{P}_t^C = P_t^C + \alpha_t^C(\mathbf{1}^T\xi_t), \forall t \tag{6b}$$

$$\tilde{P}_t^{HP} = P_t^{HP} + \alpha_t^H(\mathbf{1}^T\xi_t), \forall t \tag{6c}$$

$$\tilde{H}_t^{HS} = H_t^{HS} + \beta_t^{HS}(\mathbf{1}^T\xi_t), \forall t \tag{6d}$$

$$\tilde{T}_{n,t}^S = T_{n,t}^S + \gamma_{n,t}^S(\mathbf{1}^T\xi_t), \forall n \in \Lambda^N, \forall t \tag{6e}$$

$$\tilde{T}_{n,t}^R = T_{n,t}^R + \gamma_{n,t}^R(\mathbf{1}^T\xi_t), \forall n \in \Lambda^N, \forall t \tag{6f}$$

$$\tilde{T}_{p,t}^{S,start} = T_{p,t}^{S,start} + \gamma_{p,t}^{S,start}(\mathbf{1}^T\xi_t), \forall p \in \Lambda^P, \forall t \tag{6g}$$

$$\tilde{T}_{p,t}^{S,end} = T_{p,t}^{S,end} + \gamma_{p,t}^{S,end}(\mathbf{1}^T\xi_t), \forall p \in \Lambda^P, \forall t \tag{6h}$$

$$\tilde{T}_{p,t}^{R,start} = T_{p,t}^{R,start} + \gamma_{p,t}^{R,start}(\mathbf{1}^T\xi_t), \forall p \in \Lambda^P, \forall t \tag{6i}$$

$$\tilde{T}_{p,t}^{R,end} = T_{p,t}^{R,end} + \gamma_{p,t}^{R,end}(\mathbf{1}^T\xi_t), \forall p \in \Lambda^P, \forall t \tag{6j}$$

In (6a)-(6j), the first part of each equation is a day-ahead schedule for the forecasted wind power, where the second part is a real-time regulation action in the presence of forecast error ξ_t. The affine control polices respond to the net deviation from point forecasts of all wind farms $\mathbf{1}^T\xi_t$ in the time period t. In this way, the dimension of the uncertainty does not affect the size of the optimization problem, neither the number of decision variables nor the number of constraints. We define $\alpha_t^G \in \mathbb{R}^G$ as a participation factor of the conventional generation units to handle the unforeseen forecast errors. Whereas $\alpha_t^C \in \mathbb{R}^{N^c}$, $\alpha_t^H \in \mathbb{R}^{N^h}$ are participation factors of the CHP units and HPs. In order to utilize the flexibility of the DHS, the participation factors of the heat suppliers against forecast errors is introduced as $\beta_t^{HS} \in \mathbb{R}^{N^{HS}}$. Under CF-VT control strategy DHS temperatures are controllable at each node. Variables $\gamma_t^S, \gamma_t^R \in \mathbb{R}^N$ and $\gamma_t^{S,start}, \gamma_t^{S,end}, \gamma_t^{R,start}, \gamma_t^{R,end} \in \mathbb{R}^P$ represent the changes in the nodal temperatures in response to the uncertainty of wind power in real time.

The real-time forecast errors transform constraint (1a) into

$$\begin{aligned}&\mathbf{1}^T(P_t^G + \alpha_t^G(\mathbf{1}^T\xi_t)) + \mathbf{1}^T(P_t^C + \alpha_t^C(\mathbf{1}^T\xi_t)) + \mathbf{1}^T(P_t^f - \xi_t)\\ &= \mathbf{1}^T P_t^D + \mathbf{1}^T(P_t^{HP} + \alpha_t^H(\mathbf{1}^T\xi_t)), \forall t\end{aligned} \tag{7}$$

By matching the zero- and first-order coefficients of ξ_t on both sides of (7) [44], the deterministic part of the constraint remains unchanged as (1a) and we require

$$\mathbf{1}^T\alpha_t^G + \mathbf{1}^T\alpha_t^C - \mathbf{1}^T\alpha_t^H = 1, \forall t \tag{8}$$

Similarly, the same technique for each equality constraint that consists of stochastic variables is used to derive

$$\alpha_{s,t}^{HS} = Cm_{s,t}^{HS}\left(\gamma_{n,t}^S - \gamma_{n,t}^R\right), \forall n \in \Lambda^N, \forall s \in \Theta_n^{HS}, \forall t \tag{9a}$$

$$0 = \left(\gamma_{n,t}^S - \gamma_{n,t}^R\right), \forall n \in \Lambda^N, \forall l \in \Theta_n^{HL}, \forall t \tag{9b}$$

$$\begin{aligned}\sum_{p\in\Theta_n^{P,IN}} m_{p,t}^S\gamma_{p,t}^{S,end} &= \gamma_{n,t}^S \sum_{p\in\Theta_n^{P,IN}} m_{p,t}^S,\ \forall n \in \Lambda^N, \forall t\\ \sum_{p\in\Theta_n^{P,OUT}} m_{p,t}^R\gamma_{p,t}^{R,end} &= \gamma_{n,t}^R \sum_{p\in\Theta_n^{P,OUT}} m_{p,t}^R,\ \forall n \in \Lambda^N, \forall t\end{aligned} \tag{9c}$$

$$\begin{aligned}\gamma_{n,t}^S &= \gamma_{p,t}^{S,start},\ \forall n \in \Lambda^N,\ \forall p \in \Theta_p^{P,OUT}, \forall t\\ \gamma_{n,t}^R &= \gamma_{p,t}^{R,start},\ \forall n \in \Lambda^N,\ \forall p \in \Theta_p^{P,IN}, \forall t\end{aligned} \tag{9d}$$

$$\begin{aligned}\gamma_{n,t}^S &= \gamma_{p,t}^{S,end},\ \forall n \in \Lambda^{N-},\ \forall p \in \Theta_p^{P,IN}, \forall t\\ \gamma_{n,t}^R &= \gamma_{p,t}^{R,end},\ \forall n \in \Lambda^{N+},\ \forall p \in \Theta_p^{P,OUT}, \forall t\end{aligned} \tag{9e}$$

$$\begin{aligned}\gamma_{p,t}^{S,end} &= \gamma_{p,t-\tau_{p,t}^S}^{S,start}(1 - \tfrac{2\lambda_p}{C\rho R_p}\tau_{p,t}^S), \forall p \in \Lambda^P, \forall t\\ \gamma_{p,t}^{R,end} &= \gamma_{p,t-\tau_{p,t}^R}^{R,start}(1 - \tfrac{2\lambda_p}{C\rho R_p}\tau_{p,t}^R), \forall p \in \Lambda^P, \forall t\end{aligned} \tag{9f}$$

$$\beta_{s,t}^{H} = COP_s \alpha_{s,t}^{H},\ \forall s \in \Theta_n^{HP}, \forall t \tag{9g}$$

In the proposed model the inequality constraints are replaced by distributionally robust chance-constraints as follows

$$\begin{aligned}\min_{\mathbb{P}_\xi \in \mathcal{D}_{\xi_t}} \mathbb{P}(&C_k^G \tilde{P}_t^G + C_k^W (P_t^f - \xi_t) + C_k^C \tilde{P}_t^C \\ &- C_k^D P_t^D - C_k^{HP} \tilde{P}_t^{HP} \leq P_k^L) \geq 1 - \epsilon_k, \forall t, \forall k\end{aligned} \tag{10a}$$

$$\begin{aligned}\min_{\mathbb{P}_\xi \in \mathcal{D}_{\xi_t}} \mathbb{P}(&C_k^G \tilde{P}_t^G + C_k^W (P_t^f - \xi_t) + C_k^C \tilde{P}_t^C \\ &- C_k^D P_t^D - C_k^{HP} \tilde{P}_t^{HP} \geq -P_k^L) \geq 1 - \epsilon_k, \forall t, \forall k\end{aligned} \tag{10b}$$

$$\min_{\mathbb{P}_\xi \in \mathcal{D}_{\xi_t}} \mathbb{P}(\tilde{P}_{i,t}^G \leq \overline{P}_i^G) \geq 1 - \epsilon_i, \forall t, \forall i \tag{10c}$$

$$\min_{\mathbb{P}_\xi \in \mathcal{D}_{\xi_t}} \mathbb{P}(\tilde{P}_{i,t}^G \geq \underline{P}_i^G) \geq 1 - \epsilon_i, \forall t, \forall i \tag{10d}$$

$$\min_{\mathbb{P}_\xi \in \mathcal{D}_{\xi_t}} \mathbb{P}(\tilde{P}_{i,t}^G - \tilde{P}_{i,t-1}^G \leq \overline{R}_i^G) \geq 1 - \epsilon_i, \forall i, \forall t+1 \tag{10e}$$

$$\min_{\mathbb{P}_\xi \in \mathcal{D}_{\xi_t}} \mathbb{P}(\tilde{P}_{i,t-1}^G - \tilde{P}_{i,t}^G \leq \underline{R}_i^G) \geq 1 - \epsilon_i, \forall i, \forall t+1 \tag{10f}$$

$$\min_{\mathbb{P}_\xi \in \mathcal{D}_{\xi_t}} \mathbb{P}(\tilde{P}_{s,t}^C - \tilde{P}_{s,t-1}^C \leq \overline{R}_s^C) \geq 1 - \epsilon_s, \forall s \in \Theta_n^{CHP}, \forall t+1 \tag{10g}$$

$$\min_{\mathbb{P}_\xi \in \mathcal{D}_{\xi_t}} \mathbb{P}(\tilde{P}_{s,t-1}^C - \tilde{P}_{s,t}^C \leq \underline{R}_s^C) \geq 1 - \epsilon_s, \forall s \in \Theta_n^{CHP}, \forall t+1 \tag{10h}$$

$$\min_{\mathbb{P}_\xi \in \mathcal{D}_{\xi_t}} \mathbb{P}(\tilde{H}_{s,t}^{HS} \leq \overline{H}_s^{HS}) \geq 1 - \epsilon_s, \forall s \in \Theta_n^{HS}, \forall t \tag{10i}$$

$$\min_{\mathbb{P}_\xi \in \mathcal{D}_{\xi_t}} \mathbb{P}(\tilde{H}_{s,t}^{HS} \geq \underline{H}_s^{HS}) \geq 1 - \epsilon_s, \forall s \in \Theta_n^{HS}, \forall t \tag{10j}$$

$$\min_{\mathbb{P}_\xi \in \mathcal{D}_{\xi_t}} \mathbb{P}(\tilde{T}_{n,t}^S \leq \overline{T}_n^S) \geq 1 - \epsilon_n,\ \forall n \in \Lambda^N, \forall t \tag{10k}$$

$$\min_{\mathbb{P}_\xi \in \mathcal{D}_{\xi_t}} \mathbb{P}(\tilde{T}_{n,t}^S \geq \underline{T}_n^S) \geq 1 - \epsilon_n,\ \forall n \in \Lambda^N, \forall t \tag{10l}$$

$$\min_{\mathbb{P}_\xi \in \mathcal{D}_{\xi_t}} \mathbb{P}(\tilde{T}_{n,t}^R \leq \overline{T}_n^R) \geq 1 - \epsilon_n,\ \forall n \in \Lambda^N, \forall t \tag{10m}$$

$$\min_{\mathbb{P}_\xi \in \mathcal{D}_{\xi_t}} \mathbb{P}(\tilde{T}_{n,t}^R \geq \underline{T}_n^R) \geq 1 - \epsilon_n,\ \forall n \in \Lambda^N, \forall t \tag{10n}$$

$$\min_{\mathbb{P}_\xi \in \mathcal{D}_{\xi_t}} \mathbb{P}(\tilde{P}_{s,t}^C \geq r_s \tilde{H}_{s,t}^{HS}) \geq 1 - \epsilon_s,\ \forall s \in \Theta_n^{CHP}, \forall t \tag{10o}$$

$$\min_{\mathbb{P}_\xi \in \mathcal{D}_{\xi_t}} \mathbb{P}(\rho_s^E \tilde{P}_{s,t}^C + \rho_s^H \tilde{H}_{s,t}^{HS} \leq \overline{F}_s) \geq 1 - \epsilon_s,\ \forall s \in \Theta_n^{CHP}, \forall t \tag{10p}$$

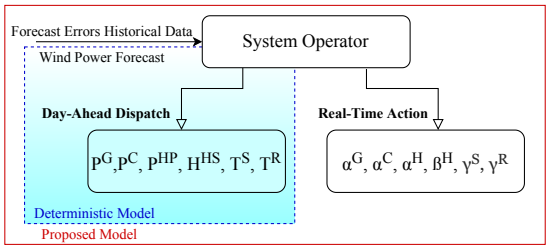

Figure 2: Comparison between deterministic and proposed DRCC model.

$$\min_{\mathbb{P}_\xi \in \mathcal{D}_{\xi_t}} \mathbb{P}(\rho_s^E \tilde{P}_{s,t}^C + \rho_s^H \tilde{H}_{s,t}^{HS} \geq 0) \geq 1 - \epsilon_s, \ \forall s \in \Theta_n^{CHP}, \forall t \tag{10q}$$

where parameter $\epsilon_{(.)} \geq 0$ is a violation probability, and $1 - \epsilon_{(.)}$ is referred as a confidence level. $\mathbb{P}(.)$ is the probability operator over the uncertain variable ξ_t. In this way, the probability of meeting chance constraints enforced to be greater or equal than the confidence level. Distributionally robust (DR) formulation makes no assumption on probability distribution and enforces constraints to hold for the worst-case distribution $\mathbb{P}_\xi$ from the ambiguity set $\mathcal{D}_{\xi_t}$ of all distributions with the same mean μ_t and covariance Σ_t. Thus, the objective function is

$$\min_{\tilde{\Xi}} \max_{\mathbb{P}_\xi \in \mathcal{D}_\xi} \mathbb{E}_{\mathbb{P}_\xi}[\sum_t (c^g)^T \tilde{P}_t^G + (c^e)^T \tilde{P}_t^C + (c^h)^T \tilde{H}_t^{HS}] \tag{11}$$

which minimizes the total worst-case expected cost over the worst distribution $\mathbb{P}_\xi$ from the ambiguity set $\mathcal{D}_{\xi_t}$.

$$\tilde{\Xi} = \{\tilde{T}_{p,t}^{S,start}, \tilde{T}_{p,t}^{S,end}, \tilde{T}_{p,t}^{R,start}, \tilde{T}_{p,t}^{R,end}, \tilde{T}_{n,t}^S, \tilde{T}_{n,t}^R, \tilde{H}_{s,t}^{HS}, \tilde{P}_t^C, \tilde{P}_t^{HP}, \tilde{P}_t^G\}$$

In this regard, the uncertainty-aware problem, which is formulated with stochastic variables and probabilistic chance-constraints, is a one-stage stochastic program. The comparison between the deterministic and the proposed model DRCC is shown in Fig. 2. In order to solve the proposed DRCC model, a computationally tractable reformulations have to be employed.

4. Distributionally Robust Reformulation

4.1. Distributionally Robust Chance Constraints

Theorem 2.2 in [45] derives the exact second-order cone analytical reformulation of individual DR chance-constraints given the first and second-order moment information. Each chance constraint could be written in the following form

$$\min_{\mathbb{P}_{\xi_t} \in \mathcal{D}_{\xi_t}} \mathbb{P}(A_{j,t}^T \xi_t \leq b_{j,t}) \geq 1 - \epsilon_j, \forall j = 1 \dots m, \forall t$$

where m is a number of chance constraints. Assuming $\mu_t = 0$, it is equivalent to

$$\sqrt{\left(\frac{1-\epsilon_j}{\epsilon_j}\right) A_{j,t}^T(\Sigma_t) A_{j,t}} \leq b_{j,t},\ \forall j = 1 \dots m, \forall t$$

Interested readers may refer to [30], where the derivation procedure for the chance-constrained optimal power flow problem is shown. The previous inequality is a second-order cone constraint and we rewrite it as

$$K_{\epsilon_j} ||A_{j,t}(\Sigma_t)^{\frac{1}{2}}||_2 \leq b_{j,t},\ \forall j, \forall t \tag{12}$$

where $K_{\epsilon_j} = \sqrt{\left(\frac{1-\epsilon_j}{\epsilon_j}\right)}$. For example, constraint (10a) is reformulated as

$$\begin{aligned} &K_{\epsilon_k} ||(C_k^G \alpha_t^G \mathbf{1}^T + C_k^C \alpha_t^C \mathbf{1}^T - C_k^W - C_k^{HP} \alpha_t^H \mathbf{1}^T) \Sigma_t^{\frac{1}{2}}||_2 \leq P_k^L \\ &- (C_k^G P_t^G + C_k^C P_t^C + C_k^W P_t^f - C_k^D P_t^D - C_k^{HP} P_t^{HP}), \forall k, \forall t \end{aligned} \tag{13}$$

Similarly, the rest of the chance-constraints are expressed in terms of affine control polices as second-order cone constraints. Note that inter-temporal ramping constraints (10e)-(10h) are reformulated with the following uncertainty

$$\hat{\xi}_t = \begin{bmatrix} \xi_t \\ \xi_{t-1} \end{bmatrix}$$

and covariance matrix therefore is

$$\hat{\Sigma}_t = \begin{bmatrix} \Sigma_t & \Sigma_{t,t-1} \\ \Sigma_{t,t-1} & \Sigma_{t-1} \end{bmatrix}$$

where $\hat{\xi}_t \in \mathbb{R}^{2W}$ is a stacked inter-temporal forecast error vector, and $\hat{\Sigma}_t \in \mathbb{R}^{2W \times 2W}$ its covariance matrix, which also includes the temporal correlation between the neighbouring hours t and $t-1$ [33].

4.2. Reformulation with Gaussian distribution

[46] shows that under the assumption, that uncertainty follows Gaussian distribution with $\mu_t = 0$, a chance-constraint can be reformulated as a second-order cone constraint

$$\Psi^{-1}(1-\epsilon_j) ||A_{j,t}^T(\Sigma_t)^{\frac{1}{2}}||_2 \leq b_{j,t},\ \forall j, \forall t \tag{14}$$

where $\Psi^{-1}(.)$ is the normal inverse cumulative distribution function. The value of K_{ϵ_j} in the distributional robust case is higher than $\Psi^{-1}(1-\epsilon_j)$ for the same violation probability ϵ_j. Hence, DR chance-constraints are tighter and provide a more robust and conservative solution, than their Gaussian reformulation.

4.3. Objective Function

Objective function (11) is written as,

$$\min_{\tilde{\Xi}} \max_{\mathbb{P}_\xi \in \mathcal{D}_\xi} \mathbb{E}_{\mathbb{P}_\xi}[\sum_t (c^g)^T(P_t^G + \alpha_t^G(\mathbf{1}^T\xi_t)) + (c^e)^T(P_t^C + \alpha_t^C(\mathbf{1}^T\xi_t)) + (c^h)^T(H_t^{HS} + \beta_t^{HS}(\mathbf{1}^T\xi_t))] \tag{15}$$

and has a min-max structure such that the total system dispatch cost is minimized, while the uncertain variable ξ_t that is drawn from probability distribution $\mathbb{P}_\xi \in \mathcal{D}_\xi$ maximizes the cost of dispatch. We assume that the mean of the forecast error vector is zero, i.e.,

$$\mathbb{E}_{\mathbb{P}_\xi}[\xi_t] = \mu_t = 0, \forall t$$

Decision variables P_t^G, P_t^C, H_t^{HS} do not depend on the uncertainty ξ_t and are constants for the expectation operator $\mathbb{E}_{\mathbb{P}_\xi}[.]$. Henceforth in the resulting objective function ξ_t does not exist and operator $\max_{\mathbb{P}_\xi \in \mathcal{D}_\xi}$ could be removed. Finally, the objective function has the same form (4), as in a deterministic model. The resulting model is a SOCP and presented in Appendix A. It is convex and therefore could be directly solved by the commercial optimization packages.

5. Case study

5.1. Test System

District heating in Denmark consists of numerous independent DH grids that are not interconnected. However, there are large DH grids in the big cities: Copenhagen, Aarhus, Odense, and Aalborg. A practical example of such IEHS could be the district heating system in Aarhus. Aarhus is one of the biggest cities in Denmark with a total of 350,000 customers. A giant extraction CHP plant in Studstrup serves a centralized DH area [47]. The CHP has two large-scale units, they are 350 MW of each and the transmission level voltage is 400 kV.

We study the model on the modified integrated six-bus EPS and seven-node DHS and it is shown in Fig. 3. The system consists of two wind power plants with a rated capacity of 100 MW and two gas-turbine generators G1 and G2. In the power system the base power is 100 MVA and the base voltage is 345 kV. The overall system wind power forecast is depicted in Fig. 4a. The electrical (left vertical axis) and heat (right vertical axis) demand are taken from [11] and shown in Fig. 4b respectively. Technical parameters of generation units, transmission network, and DHN are presented in Appendix B. The model is simulated over 24 hours with a one-hour time resolution. 10000 wind power historical samples for 2 wind farms from [33] is used. We use first 5000 trajectories to calculate mean production of the wind farms P_t^f. The wind power forecast errors samples are generated as in [48] and used to compute covariance matrices Σ_t, $\hat{\Sigma}_t$. The rest 5000 trajectories are test data to perform out-of-sample

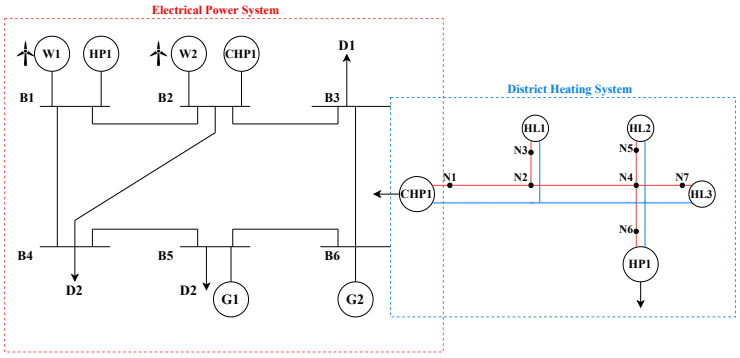

Figure 3: Configuration of the six-bus and seven-node integrated system.

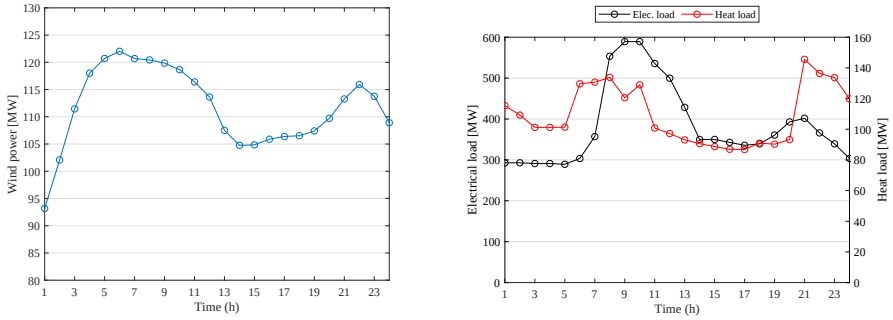

(a) Wind power forecasts

(b) Demand curves

Figure 4: Wind power and demand curves

analysis. We also assume that each chance-constraint has the same value of the violation probability parameter, i.e. $\epsilon_j = \epsilon$ for every j. In this study water density is $\rho = 1000$ kg/m^3 and thermal loss coefficient $\lambda_p = 0.2\ J \times m^{-2} \times s^{-2}/K$. The simulation is run in MATLAB on a personal computer with 3.4 GHz Intel Core i5 processor and 8GB memory using YALMIP interface [49] with Mosek solver [50]. The CPU time for the DRCC model varies from 17 to 20 seconds, depending on the values of ϵ_j, whereas the deterministic model took 6 seconds to run.

5.2. IEHS dispatch under different models

To validate the effectiveness of the proposed DRCC dispatch scheme, the traditional deterministic dispatch and chance-constrained dispatch are conducted for a comprehensive comparison. Three cases are set. Case 1 is deterministic scheduling, where the uncertainty was not taken into account. Case 2 considers the short-term uncertainty of the wind power plants, but with an assumption, that it follows a Gaussian probability distribution. Hence, no ambiguity set (5) is used and all the chance-constraints were reformulated analytically by (14).

Table 1: Cost performance, $\epsilon = 0.05$

	Case 1	Case 2	Case 3
Total operational cost [$]	228,387	229,004	232,541
Fuel consumption of CHP [MW× h]	11,900	11,800	11,017

Case 3 is based on the DRCC dispatch model, where no assumption was made about the probability distribution of the uncertain parameter.

In Table 1 system operational cost and fuel consumption of the CHP are presented. For Case 2 and Case 3, violation probability ϵ is set to 5% for each chance constraint. The value of K_ϵ in Case 2 is 1.645 and 4.359 in Case 3. From Table 1 we can conclude that the system operation cost is the lowest in the deterministic case, whereas the fuel consumption of the CHP is the highest. The system cost increases when the uncertainty is considered. In Case 2, the cost went up by 0.27 % when assuming that uncertainty is Gaussian, while in Case 3 by 1.82 %. The system cost increased due to the ability to balance the uncertainty in real-time and therefore improved system security level. The detailed comparison of the cost between Gaussian reformulation and distributionally robust reformulation is discussed in Section 5.3. Compared to Case 1, the CHP fuel consumption went down by 0.8 % in Case 2 and by 7,42 % in Case 3. Hence it shows that there is less usage of the CHP in the day-ahead stage, when the uncertainty is taken into account. These findings are consistent with that shown in Fig. 5 and Fig. 6.

In Fig. 5, the day-ahead dispatch of all power generation units is presented. It demonstrates that more expensive units are scheduled when the uncertainty is considered to improve system security. We can see that from hour 1 to hour 6, the CHP power output is reduced, while unit G1 power is rising. Moreover, when the electrical demand is going up during peak-hours, the most expensive unit G2 is scheduled at 8 hour in Case 2 with respect to Case 1, and at 10-11 hour in Case 3. The increment of the electrical power from the G1 and G2 leads to the higher system operational cost. These units have to be dispatch more, so the flexibility of the DHS could be utilized and provide sufficient real-time regulation.

The reduction of the CHP power output is reducing the fuel consumption of the CHP. It can be observed from Fig. 6, that compared with Case 1, in the proposed models CHP operated more securely. For example, during 1-3 hours, heat and power from CHP unit in Case 1 scheduled at its maximum capability, while it was less tight in Case 2 and even less tight in Case 3. This allows the model to adjust the operating point of the CHP unit within its feasible region in real-time and provide needed regulation with affine policies. It can be seen that, compared to Case 2, in Case 3 CHP unit operated at the upper bound of the fuel consumption only between 8-13 hours to supply electrical load during peak-hours and at 21 hour, when the heat demand has the highest point. Thus, it can be concluded that Case 3 ensures less risky operation of the CHP plant against the renewable energy source uncertainty.

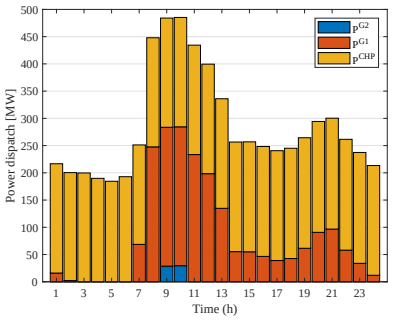

(a) Case 1

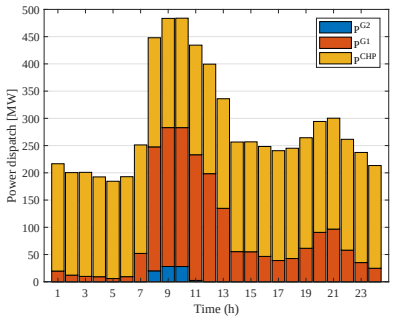

(b) Case 2

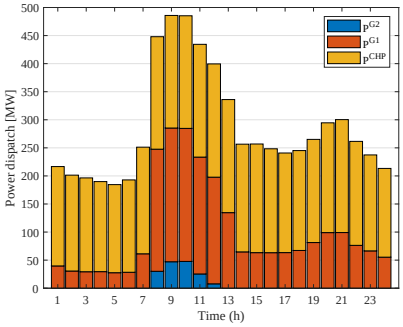

(c) Case 3

Figure 5: Power dispatch in 3 cases.

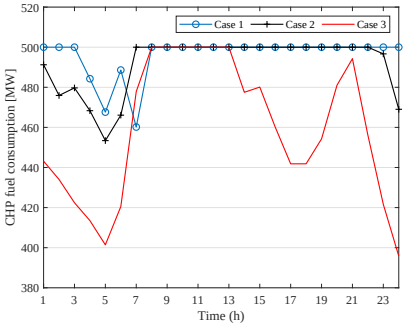

Figure 6: CHP fuel consumption in 3 cases

In this subsection it is indicated that to exploit the flexibility of the DHS and provide regulation in real-time, the wind uncertainty has to be modeled to ensure the reliable operation of the district heating units.

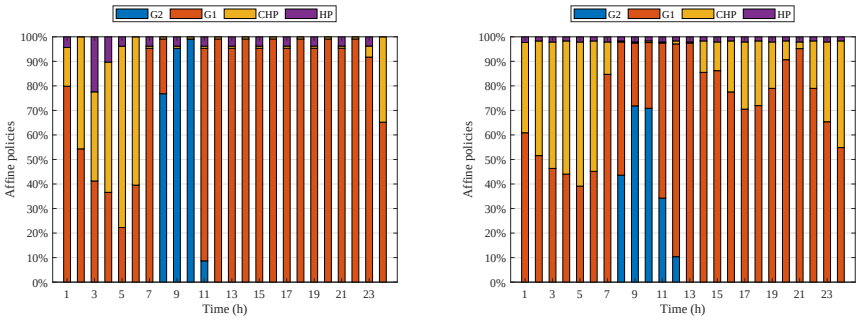

(a) Case 2 (b) Case 3

Figure 7: Participation factor in different distribution assumptions

5.3. Analysis of Distributional Robustness

In this subsection, the robustness of the decisions of the proposed DRCC model is analyzed by performing out-of-sample analysis. We consider Case 2 and Case 3 only, since only they account for the wind power uncertainty. After solving the model for 24 operating hours we fix the obtained decision variables for every hour. Using 5000 out-of-sample wind power trajectories, for every realization of the wind power output, we compute the actual power and heat of the generation units, power flows in the transmission lines, temperatures in the DHS nodes. Further we investigate if the chance-constraints are violated and calculate ex-ante violation probabilities with the procedure described in [33].

Fig. 7 shows the share of the participation factors in the EPS under different distribution assumptions. It can be seen that assuming different distributions changes the pattern of the obtained affine policies. For instance, during 14-23 hours, compared to Case 2, in Case 3 the CHP unit increases its participation to hedge the wind power uncertainty, and therefore it is less scheduled in the day-ahead stage. Furthermore, it could be observed that the share of the participation factors for the unit G1 and G2 is reduced when the system robustness is increasing. The value of K_ϵ is higher in Case 3 and therefore the proposed DRCC model behaves more conservatively in real-time, not allowing the abrupt changes in the power output of the generation units in real-time.

To utilize DHS flexibility in real-time, the system operator needs to reserve not only electrical power capacity but also thermal capacity in the DHS. Fig. 8 shows the participation factors of the CHP unit and HP on the heating side due to the interconnection between the EPS and DHS. The left-sidebar shows the factors for Case 2, and the right-sidebar represents participation factors for Case 3. It can be found that assuming no distribution in Case 3 leads to the less risky solutions since the affine policies for the heat side are considerably less than in Case 2. It allows the CHP unit to stay in the feasible operation region while providing real-time balancing.

Out-of-sample analysis lets us see how the affine policies work in real-time. For example, in Fig. 9, the actual power realization of the G1 unit is shown for

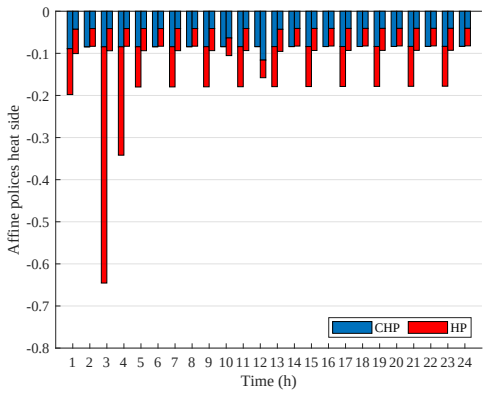

Figure 8: Affine policies of heat suppliers. Right-side bars represent Case 2. Left-side bars obtained from Case 3

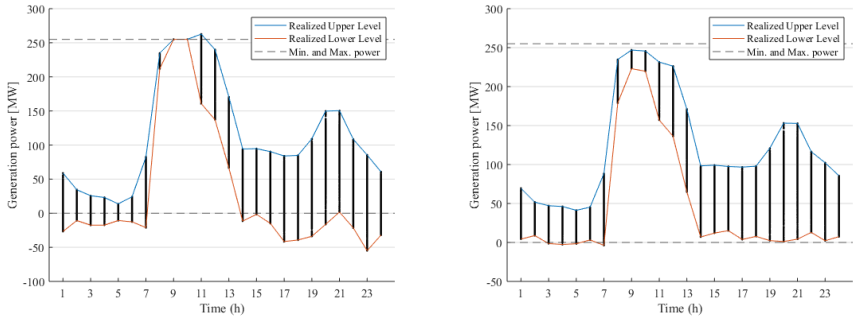

(a) Case 2 (b) Case 3

Figure 9: Out-of-sample Gen1 power output under different robustness

two cases. Black dots represent G1 power when the actual wind power output is considered. The blue and red lines are the maximum and minimum realizations respectively. The dashed lines are the upper and lower bounds of G1 unit power output. In terms of Case 2, the actual power generation G1 in Case 3 is within the bounds, and generator limits are violated slightly, in 0.14 % realizations. Hence the system is operating more reliably, compared to Case 2, where the ex-ante probability to violate the constraint is 8.9 % and it yields more risks in the actual operation. Eventually, the DRO case obtains a more reliable solution but the system operation cost is higher.

Fig. 10 demonstrates the system cost of the day-ahead plotted versus confidence level. In can be observed, that increasing system security level scarifies the system cost for both cases. The more robust decisions obtained the more costly system operation is. Compared to Case 2, the system operating cost of Case 3 is higher for all the confidence levels. However, it shows a much better

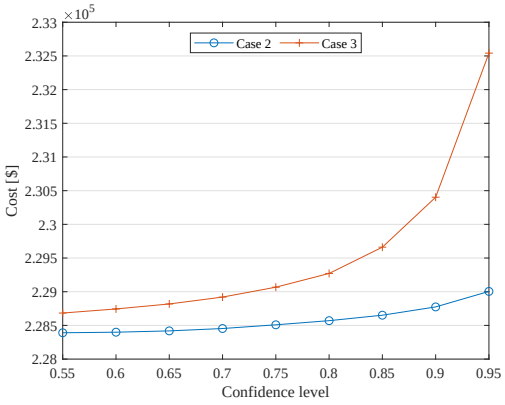

Figure 10: Total system cost

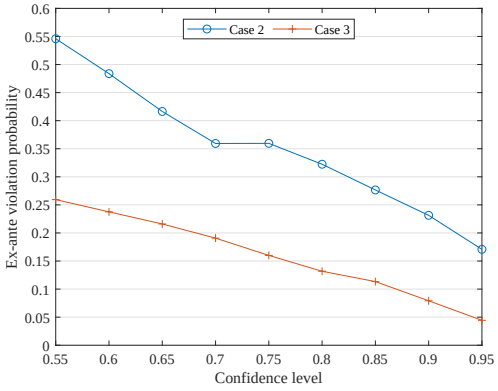

Figure 11: Ex-ante violations probabilities

out-of-sample performance. This can be seen in Fig. 11. It also shows that empirical violation probabilities in Case 3 are always less than assumed theoretical ones.

Table 2 gives quantitative comparisons of Case 3 empirical ex-ante violation probabilities by constraint type. It can be found that CHP and generator ramp constraints violated at most. However, even at $\epsilon = 0.25$, Case 3 model performs much better than expected, with CHP ramp violation probability 0.16. In contrast, the line limits and heat stations limits constraints are satisfied even at $\epsilon = 0.25$. By doing such an analysis, the system operator can adjust the value of ϵ, and therefore K_ϵ, for every type of constraint to reduce the conservativeness of the decisions and, as a result, the system operating cost.

Table 2: Empirical violation probabilities for every constraint type

Constraint type	$\epsilon = 0.05$	$\epsilon = 0.15$	$\epsilon = 0.25$
CHP region	0	0.0056	0.0356
HS limits	0	0	0
G limits	0.0014	0.0408	0.0846
Line limits	0	0	0
CHP ramping	**0.0440**	0.0440	0.0340
G ramping	0	**0.1134**	**0.16**
T^R limits	0	0.0056	0.0682
T^S limits	0	0.0050	0.0434

Table 3: Cost performance, $\epsilon = 0.05$

	Case 3	Case 4
Total operational cost [$]	232,541	236,339
Fuel consumption of CHP [MW× h]	11,017	9,940

5.4. Cost benefits of DHS flexibility

In order to validate the cost-effectiveness of the proposed DRCC model in providing additional flexibility, a comparison between Case 3 and Case 4 is performed. In Case 4, the flexibility of the DHS is not taken into account. Affine policies are allocated only to conventional generator units and therefore, all the constraints with district heating variables are treated as deterministic constraints. It can be seen, from Table 3, when the DHS does not provide regulation in real-time, the system operating cost increased by 1.6 %. The reason for that is more expensive conventional generator units are providing down regulation in case of high actual wind power, and henceforth they are dispatch more in the day-ahead stage. This is proved by the fact, that CHP fuel consumption decreased in Case 4 by 9.77%.

5.5. Practical application

The system operators respond to the real-time deviation of actual wind or other renewable energy sources power from the forecasted values by activating the balancing reserves. Traditionally, the system operators define the amounts of the reserves based on the experience. The proposed model gives the possibility to define the amount of the reserves implicitly in a data-driven manner with the framework of [30, 51].

In practice, the DHS and EPS are owned by different entities, and they are controlled by different operators. Due to privacy issues, it is not practical to exchange detailed information about operation states between the EPS and DHS operators. Therefore, the DHS and EPS should be dispatched separately and a decentralized solution to the coordination problem should be proposed. A decentralized solution to the proposed DRCC model may be achieved using optimality condition decomposition (OCD). In [52], the OCD algorithm is applied to

solve the decentralized coordination of EPS and DHS considering the pipelines energy storage in the district heating network. In order to implement the OCD algorithm in the proposed DRCC, several adjustments to the formulation need to be done. The feasible operation region of the CHP can be represented using a convex polyhedron with extreme points [53]. A virtual tie-line between the EPS and the DHS has to be introduced and, since the uncertainty is considered in the DRCC, the participation factor of the virtual tie-line to mitigate the uncertainty should be also defined. The proposed DRCC model is a convex SOCP; hence, the OCD algorithm applied to the proposed model is guaranteed to converge to the optimal point.

We leave the extensions for the future works.

6. Conclusion

This paper proposes a distributionally robust optimization dispatch scheme for the IEHS considering wind power uncertainty. First, to ensure the secure operation and flexibility provision by the DHS, the real-time regulation actions to the uncertain wind power generation is modeled in the electricity and heat side. Furthermore, the stochastic program is reformulated into a convex SOCP using a moment-based ambiguity set. The proposed DRCC model outperforms a deterministic dispatch and the chance-constrained model based on Gaussian distribution in ensuring secure operation of the system. Out-of-sample analysis conducted on a case study demonstrates that the proposed DRCC model maintains better reliable functioning of both the EPS and DHS.

Future work needs to investigate the possibility of different CHP units, for example back-pressure steam turbines, to provide flexibility in the proposed scheme. The amount of balancing reserves provided by HPs is also an interesting topic for future studies. Moreover, the other methods of the ambiguity sets construction and their influence on the resource actions should also be explored.

Acknowledgment

This work was supported in part by the EUDP programme through the SMART MLA project (grant no 64018-0302) and in part by DTU through the Alliance PhD scholarship.

References

[1] H. Lund, B. Möller, B. V. Mathiesen, A. Dyrelund, The role of district heating in future renewable energy systems, Energy 35 (3) (2010) 1381–1390.

[2] H. Lund, B. V. Mathiesen, Energy system analysis of 100% renewable energy systems—the case of denmark in years 2030 and 2050, Energy 34 (5) (2009) 524–531.

[3] J. Wang, S. You, Y. Zong, C. Træholt, Z. Y. Dong, Y. Zhou, Flexibility of combined heat and power plants: A review of technologies and operation strategies, Applied energy 252 (2019) 113445.

[4] J. Wang, S. You, Y. Zong, H. Cai, C. Træholt, Z. Y. Dong, Investigation of real-time flexibility of combined heat and power plants in district heating applications, Applied energy 237 (2019) 196–209.

[5] H. Lund, Large-scale integration of wind power into different energy systems, Energy 30 (13) (2005) 2402–2412.

[6] N. Zhang, X. Lu, M. B. McElroy, C. P. Nielsen, X. Chen, Y. Deng, C. Kang, Reducing curtailment of wind electricity in china by employing electric boilers for heat and pumped hydro for energy storage, Applied Energy 184 (2016) 987–994.

[7] X. Chen, C. Kang, M. O'Malley, Q. Xia, J. Bai, C. Liu, R. Sun, W. Wang, H. Li, Increasing the flexibility of combined heat and power for wind power integration in china: Modeling and implications, IEEE Transactions on Power Systems 30 (4) (2014) 1848–1857.

[8] J. Li, J. Fang, Q. Zeng, Z. Chen, Optimal operation of the integrated electrical and heating systems to accommodate the intermittent renewable sources, Applied Energy 167 (2016) 244–254.

[9] J. Zheng, Z. Zhou, J. Zhao, J. Wang, Integrated heat and power dispatch truly utilizing thermal inertia of district heating network for wind power integration, Applied energy 211 (2018) 865–874.

[10] Z. Li, W. Wu, M. Shahidehpour, J. Wang, B. Zhang, Combined heat and power dispatch considering pipeline energy storage of district heating network, IEEE Transactions on Sustainable Energy 7 (1) (2015) 12–22.

[11] L. Mitridati, J. A. Taylor, Power systems flexibility from district heating networks, 20th Power Systems Computation Conference, PSCC 2018 (2018) 1–7doi:10.23919/PSCC.2018.8442617.

[12] S. Huang, W. Tang, Q. Wu, C. Li, Network constrained economic dispatch of integrated heat and electricity systems through mixed integer conic programming, Energy 179 (2019) 464–474.

[13] J. Kensby, A. Trüschel, J.-O. Dalenbäck, Potential of residential buildings as thermal energy storage in district heating systems–results from a pilot test, Applied Energy 137 (2015) 773–781.

[14] X. Jin, Y. Mu, H. Jia, J. Wu, T. Jiang, X. Yu, Dynamic economic dispatch of a hybrid energy microgrid considering building based virtual energy storage system, Applied energy 194 (2017) 386–398.

[15] M. Leśko, W. Bujalski, K. Futyma, Operational optimization in district heating systems with the use of thermal energy storage, Energy 165 (2018) 902–915.

[16] Y. Yang, K. Wu, H. Long, J. Gao, X. Yan, T. Kato, Y. Suzuoki, Integrated electricity and heating demand-side management for wind power integration in china, Energy 78 (2014) 235–246.

[17] W. Gu, J. Wang, S. Lu, Z. Luo, C. Wu, Optimal operation for integrated energy system considering thermal inertia of district heating network and buildings, Applied Energy 199 (2017) 234–246.

[18] P. Li, H. Wang, Q. Lv, W. Li, Combined heat and power dispatch considering heat storage of both buildings and pipelines in district heating system for wind power integration, Energies 10 (7) (2017) 893.

[19] P. Veers, K. Dykes, E. Lantz, S. Barth, C. L. Bottasso, O. Carlson, A. Clifton, J. Green, P. Green, H. Holttinen, D. Laird, V. Lehtomäki, J. K. Lundquist, J. Manwell, M. Marquis, C. Meneveau, P. Moriarty, X. Munduate, M. Muskulus, J. Naughton, L. Pao, J. Paquette, J. Peinke, A. Robertson, J. Sanz Rodrigo, A. M. Sempreviva, J. C. Smith, A. Tuohy, R. Wiser, Grand challenges in the science of wind energy, Science 366 (6464). doi:10.1126/science.aau2027.

[20] A. J. Conejo, M. Carrión, J. M. Morales, et al., Decision making under uncertainty in electricity markets, Vol. 1, Springer, 2010.

[21] M. Zugno, A. J. Conejo, A robust optimization approach to energy and reserve dispatch in electricity markets, European Journal of Operational Research 247 (2) (2015) 659–671.

[22] M. Bornapour, R.-A. Hooshmand, A. Khodabakhshian, M. Parastegari, Optimal coordinated scheduling of combined heat and power fuel cell, wind, and photovoltaic units in micro grids considering uncertainties, Energy 117 (2016) 176–189.

[23] A. Turk, Q. Wu, M. Zhang, J. Østergaard, Day-ahead stochastic scheduling of integrated multi-energy system for flexibility synergy and uncertainty balancing, Energy 196 (2020) 117130.

[24] C. Wang, B. Jiao, L. Guo, Z. Tian, J. Niu, S. Li, Robust scheduling of building energy system under uncertainty, Applied energy 167 (2016) 366–376.

[25] Z. Li, W. Wu, J. Wang, B. Zhang, Z. Taiyi, Transmission-Constrained Unit Commitment Considering Combined Electricity and District Heating Networks, IEEE Transactions on Sustainable Energy 7 (2) (2016) 480–492. doi:10.1109/TSTE.2015.2500571.

[26] J. Tan, Q. Wu, Q. Hu, W. Wei, F. Liu, Adaptive robust energy and reserve co-optimization of integrated electricity and heating system considering wind uncertainty, Applied Energy 260 (2020) 114230.

[27] Y. Shui, H. Gao, L. Wang, Z. Wei, J. Liu, A data-driven distributionally robust coordinated dispatch model for integrated power and heating systems considering wind power uncertainties, International Journal of Electrical Power & Energy Systems 104 (2019) 255–258.

[28] E. Delage, D. Kuhn, K. Natarajan, W. Wiesemann, Distributionally robust optimization, Tech. rep. (2018).

[29] M. Lubin, Y. Dvorkin, S. Backhaus, A robust approach to chance constrained optimal power flow with renewable generation, IEEE Transactions on Power Systems 31 (5) (2015) 3840–3849.

[30] Y. Zhang, S. Shen, J. L. Mathieu, Distributionally robust chance-constrained optimal power flow with uncertain renewables and uncertain reserves provided by loads, IEEE Transactions on Power Systems 32 (2) (2016) 1378–1388.

[31] X. Fang, B.-M. Hodge, H. Jiang, Y. Zhang, Decentralized wind uncertainty management: Alternating direction method of multipliers based distributionally-robust chance constrained optimal power flow, Applied Energy 239 (2019) 938–947.

[32] P. Xiong, P. Jirutitijaroen, C. Singh, A distributionally robust optimization model for unit commitment considering uncertain wind power generation, IEEE Transactions on Power Systems 32 (1) (2016) 39–49.

[33] F. Pourahmadi, J. Kazempour, C. Ordoudis, P. Pinson, S. H. Hosseini, Distributionally robust chance-constrained generation expansion planning, IEEE Transactions on Power Systems.

[34] Y. Zhou, M. Shahidehpour, Z. Wei, Z. Li, G. Sun, S. Chen, Distributionally robust unit commitment in coordinated electricity and district heating networks, IEEE Transactions on Power Systems 35 (3) (2019) 2155–2166.

[35] Y. Zhou, M. Shahidehpour, Z. Wei, Z. Li, G. Sun, S. Chen, Distributionally robust co-optimization of energy and reserve for combined distribution networks of power and district heating, IEEE Transactions on Power Systems 35 (3) (2019) 2388–2398.

[36] A. Ratha, A. Schwele, J. Kazempour, P. Pinson, S. S. Torbaghan, A. Virag, Data-driven affine policies for flexibility provision by natural gas networks to power systems, in: XXI Power Systems Computation Conference, 2019.

[37] X. Fang, H. Cui, H. Yuan, J. Tan, T. Jiang, Distributionally-robust chance constrained and interval optimization for integrated electricity and natural gas systems optimal power flow with wind uncertainties, Applied Energy 252 (2019) 113420.

[38] B. Skagestad, P. Mildenstein, District heating and cooling connection handbook, NOVEM, Netherlands Agency for Energy and the Environment, 2002.

[39] J. Wang, Z. Wei, B. Yang, Y. Yong, M. Xue, G. Sun, H. Zang, S. Chen, Two-stage integrated electricity and heat market clearing with energy stations, IEEE Access 7 (2019) 44928–44938.

[40] Y. Cao, W. Wei, L. Wu, S. Mei, M. Shahidehpour, Z. Li, Decentralized operation of interdependent power distribution network and district heating network: A market-driven approach, IEEE Transactions on Smart Grid 10 (5) (2018) 5374–5385.

[41] R. D. Christie, B. F. Wollenberg, I. Wangensteen, Transmission management in the deregulated environment, Proceedings of the IEEE 88 (2) (2000) 170–195.

[42] R. Gao, A. J. Kleywegt, Distributionally robust stochastic optimization with wasserstein distance, arXiv preprint arXiv:1604.02199.

[43] P. M. Esfahani, D. Kuhn, Data-driven distributionally robust optimization using the wasserstein metric: Performance guarantees and tractable reformulations, Mathematical Programming 171 (1-2) (2018) 115–166.

[44] C. S. Song, C. H. Park, M. Yoon, G. Jang, Implementation of ptdfs and lodfs for power system security, Journal of International Council on Electrical Engineering 1 (1) (2011) 49–53.

[45] M. R. Wagner, Stochastic 0–1 linear programming under limited distributional information, Operations Research Letters 36 (2) (2008) 150–156.

[46] G. C. Calafiore, L. El Ghaoui, On distributionally robust chance-constrained linear programs, Journal of Optimization Theory and Applications 130 (1) (2006) 1–22.

[47] D. E. Agency, El- og varmeproducerende værker fra energiproducenttællingen.
URL `https://ens.dk/service/statistik-data-noegletal-og-kort/interaktive-kort`

[48] C. Ordoudis, V. A. Nguyen, D. Kuhn, P. Pinson, Energy and reserve dispatch with distributionally robust joint chance constraints, Tech. rep., Technical University of Denmark (2018).

[49] J. Lofberg, Yalmip: A toolbox for modeling and optimization in matlab, in: 2004 IEEE international conference on robotics and automation (IEEE Cat. No. 04CH37508), IEEE, 2004, pp. 284–289.

[50] M. ApS, Mosek (2019).
URL `https://www.mosek.com/`

[51] M. Vrakopoulou, K. Margellos, J. Lygeros, G. Andersson, A probabilistic framework for reserve scheduling and N-1 security assessment of systems with high wind power penetration, IEEE Transactions on Power Systems 28 (4) (2013) 3885–3896.

[52] J. Huang, Z. Li, Q. Wu, Coordinated dispatch of electric power and district heating networks: A decentralized solution using optimality condition decomposition, Applied energy 206 (2017) 1508–1522.

[53] R. Lahdelma, H. Hakonen, An efficient linear programming algorithm for combined heat and power production, European Journal of Operational Research 148 (1) (2003) 141–151.

Appendix A

Final Model

The final model is a SOCP problem, which could be solved by commercial solvers.

$$\min_{\Xi_1} \sum_t (c^g)^T P_t^G + (c^e)^T P_t^C + (c^h)^T H_t^{HS} \tag{16a}$$

subject to: (1a),(2a), (2c)-(2f), (2h), (3b), (8)-(9g), (13)

$$\begin{aligned} &K_{\epsilon_k}||-(C_k^G\alpha_t^G\mathbf{1}^T + C_k^C\alpha_t^C\mathbf{1}^T - C_k^W - C_k^{HP}\alpha_t^H\mathbf{1}^T)(\Sigma_t)^{\frac{1}{2}}||_2 \leq \\ &P_k^L + (C_k^G P_t^G + C_k^C P_t^C + C_k^W P_t^f - C_k^D P_t^D - C_k^{HP} P_t^{HP}),\ \forall k, \forall t \end{aligned} \tag{16b}$$

$$K_{\epsilon_i}||\alpha_{i,t}^G\mathbf{1}^T(\Sigma_t)^{\frac{1}{2}}||_2 \leq \overline{P}_i^G - P_{i,t}^G,\ \forall i, \forall t \tag{16c}$$

$$K_{\epsilon_i}||-\alpha_{i,t}^G\mathbf{1}^T(\Sigma_t)^{\frac{1}{2}}||_2 \leq -\underline{P}_i^G + P_{i,t}^G,\ \forall i, \forall t \tag{16d}$$

$$K_{\epsilon_i}||\omega_{i,t}^G(\hat{\Sigma}_t)^{\frac{1}{2}}||_2 \leq \overline{R}_i^G - (P_{i,t}^G - P_{i,t-1}^G),\ \forall i, \forall t+1 \tag{16e}$$

$$K_{\epsilon_i}||-\omega_{i,t}^G(\hat{\Sigma}_t)^{\frac{1}{2}}||_2 \leq \underline{R}_i^G + (P_{i,t}^G - P_{i,t-1}^G),\ \forall i, \forall t+1 \tag{16f}$$

$$K_{\epsilon_s}||\omega_{s,t}^C(\hat{\Sigma}_t)^{\frac{1}{2}}||_2 \leq \overline{R}_s^C - (P_{s,t}^C - P_{s,t-1}^C),\ \forall s \in \Theta_n^{CHP}, \forall t+1 \tag{16g}$$

$$K_{\epsilon_s}||-\omega_{s,t}^C(\hat{\Sigma}_t)^{\frac{1}{2}}||_2 \leq \underline{R}_s^C + (P_{s,t}^C - P_{s,t-1}^C),\ \forall s \in \Theta_n^{CHP}, \forall t+1 \tag{16h}$$

$$K_{\epsilon_s}||\beta_{s,t}^C\mathbf{1}^T(\Sigma_t)^{\frac{1}{2}}||_2 \leq \overline{H}_s^{HS} - H_{s,t}^{HS}, \forall s \in \Theta_n^{HS}, \forall t \tag{16i}$$

$$K_{\epsilon_s}||-\beta_{s,t}^C\mathbf{1}^T(\Sigma_t)^{\frac{1}{2}}||_2 \leq -\underline{H}_s^{HS} - H_{s,t}^{HS}, \forall s \in \Theta_n^{HS}, \forall t \tag{16j}$$

$$K_{\epsilon_n}||\gamma_{n,t}^S\mathbf{1}^T(\Sigma_t)^{\frac{1}{2}}||_2 \leq \overline{T}_n^S - T_{n,t}^S, \forall n, \forall t \tag{16k}$$

$$K_{\epsilon_n}||-\gamma_{n,t}^S\mathbf{1}^T(\Sigma_t)^{\frac{1}{2}}||_2 \leq -\underline{T}_n^S - T_{n,t}^S, \forall n, \forall t \tag{16l}$$

$$K_{\epsilon_n}||\gamma_{n,t}^R\mathbf{1}^T(\Sigma_t)^{\frac{1}{2}}||_2 \leq \overline{T}_n^R - T_{n,t}^R, \forall n, \forall t \tag{16m}$$

$$K_{\epsilon_n}||-\gamma_{n,t}^R\mathbf{1}^T(\Sigma_t)^{\frac{1}{2}}||_2 \leq -\underline{T}_n^R - T_{n,t}^R, \forall n, \forall t \tag{16n}$$

$$K_{\epsilon_s}||-(\alpha_{s,t}^C - r_s\beta_{s,t}^C)\mathbf{1}^T(\Sigma_t)^{\frac{1}{2}}||_2 \leq P_{s,t}^C - r_s H_{s,t}^{HS},\ \forall s \in \Theta_n^{CHP}, \forall t \tag{16o}$$

$$K_{\epsilon_s}||-(\rho_s^E\alpha_{s,t}^C+\rho_s^H\beta_{s,t}^C)\mathbf{1}^T(\Sigma_t)^{\frac{1}{2}}||_2\leq\rho_s^E P_{s,t}^C+\rho_s^H H_{s,t}^{HS},\forall s\in\Theta_n^{CHP},\forall t \tag{16p}$$

$$K_{\epsilon_s}||(\rho_s^E\alpha_{s,t}^C+\rho_s^H\beta_{s,t}^C)\mathbf{1}^T(\Sigma_t)^{\frac{1}{2}}||_2\leq\overline{F}_s-(\rho_s^E P_{s,t}^C+\rho_s^H H_{s,t}^{HS}),\forall s\in\Theta_n^{CHP},\forall t \tag{16q}$$

where

$$\Xi_1=\{T_{p,t}^{S,start},T_{p,t}^{S,end},T_{p,t}^{R,start},T_{p,t}^{R,end},T_{n,t}^S,T_{n,t}^R,$$
$$H_{s,t}^{HS},P_t^C,P_t^{HP},P_t^G,\alpha_t^G,\alpha_t^C,\alpha_t^H,\beta_t^H,$$
$$\gamma_t^S,\gamma_t^R,\gamma_t^{S,start},\gamma_t^{S,end},\gamma_t^{R,start},\gamma_t^{R,end}\}$$

$$\omega_{i,t}^G=\begin{bmatrix}\alpha_{i,t}^G\mathbf{1}^T\\-\alpha_{i,t-1}^G\mathbf{1}^T\end{bmatrix}\forall i,\forall t+1$$

$$\omega_{s,t}^C=\begin{bmatrix}\alpha_{s,t}^C\mathbf{1}^T\\-\alpha_{s,t-1}^C\mathbf{1}^T\end{bmatrix},\forall s\in\Theta_n^{CHP},\forall t+1$$

Appendix B

Table 4: Generation units

		G_1	G_2	CHP_1	HP_1
$\overline{P}$	MW	255	148	208.3	-
$\underline{P}$	MW	0	0	0	-
$\underline{H}$	MW	-	-	0	10
$\overline{H}$	MW	-	-	250	150
$\overline{R}$	MW	179	148	41.66	-
$\underline{R}$	MW	179	148	41.66	-
$\overline{F}$	MW	-	-	500	-
COP	-	-	-	-	2.5
r	-	-	-	0.5	-
ρ^E	-	-	-	2.4	-
ρ^H	-	-	-	0.25	-
c_1	\$/ MWh	38.47	48.47	-	-
c_e	\$/ MWh	-	-	30	-
c_h	\$/ MWh	-	-	3	0

Table 5: Electrical transmission lines

		l_{12}	l_{14}	l_{23}	l_{24}	l_{36}	l_{45}	l_{56}
$\overline{P}_l$	MW	200	250	250	200	250	250	250
X	p.u.	0.17	0.0586	0.1	0.072	0.0625	0.16	0.085

Table 6: District Heating Pipes

		$p_{12,24,46}$	p_{23}	$p_{45,47}$
L_p	m	800	600	500
R_p	m	0.8	0.8	0.8

Table 7: District Heating Network Parameters

		$N_{1,2,4,6}$	N_3	N_5	N_7
H_l^L	% of load	0	30	30	40
$\underline{T}_n^S$	°C	90	90	90	90
$\overline{T}_n^S$	°C	120	120	120	120
$\underline{T}_n^R$	°C	25	25	25	25
$\overline{T}_n^R$	°C	60	60	60	60

Table 8: Electrical demand

	b_1	b_2	b_3	b_4	b_5	b_6
% of load	0	0	20	40	40	0